Evidence-Based Prediction of Cellular Toxicity for Amorphous Silica Nanoparticles

Martin[1,2,3,*]; Reiko Watanabe[2,3]; Kosuke Hashimoto[2]; Kazuma Higashisaka[1,4]; Yuya Haga[1]; Yasuo Tsutsumi[1,5]; Kenji Mizuguchi[1,2,3,*]

[1]Graduate School of Pharmaceutical Sciences, Osaka University, 1-6 Yamadaoka, Suita, Osaka 565-0871, Japan

[2]Institute for Protein Research, Osaka University, 3-2 Yamadaoka, Suita, Osaka 565-0871, Japan

[3]Artificial Intelligence Centre for Health and Biomedical Research, National Institutes of Biomedical Innovation, Health and Nutrition (NIBIOHN), 7-6-8, Saito-Asagi, Ibaraki, Osaka 567-0085, Japan

[4]Institute for Advanced Co-Creation Studies, Osaka University, 1-6 Yamadaoka, Suita, Osaka 565-0871, Japan

[5]Global Center for Medical Engineering and Informatics, Osaka University, 2-2 Yamadaoka, Suita, Osaka 565-0871, Japan

ORCID ID

Martin: 0000-0002-5286-4703

Reiko Watanabe: 0000-0001-9359-8731

Kosuke Hashimoto: 0000-0003-3031-0635

Kazuma Higashisaka: 0000-0001-9473-8302

Yuya Haga: 0000-0003-4148-2256

Yasuo Tsutsumi: -

Kenji Mizuguchi: 0000-0003-3021-7078

Abstract

Developing a generalized model for a robust prediction of nanotoxicity is critical for designing safe nanoparticles. However, complex toxicity mechanisms of nanoparticles in biological environments, such as biomolecular corona formation, prevent a reliable nanotoxicity prediction. This is exacerbated by the potential evaluation bias caused by internal validation, which is not fully appreciated. Herein, we propose an evidence-based prediction method for distinguishing between cytotoxic and noncytotoxic nanoparticles at a given condition by uniting literature data mining and machine learning. We illustrate the proposed method for amorphous silica nanoparticles (SiO_2-NPs). SiO_2-NPs are currently considered a safety concern; however, they are still widely produced and used in various consumer products. We generated the most diverse attributes of SiO_2-NP cellular toxicity to date, using >100 publications and built predictive models, with algorithms ranging from linear to nonlinear (deep neural network, kernel, and tree-based) classifiers. These models were validated using internal (4124-sample) and external (905-sample) datasets. The resultant categorical boosting (CatBoost) model outperformed other algorithms. We then identified 13 key attributes, including concentration, serum, cell, size, time, surface, and assay type, which can explain SiO_2-NP toxicity, using the Shapley Additive exPlanation values in the CatBoost model. The serum attribute underscores the importance of nanoparticle–corona complexes for nanotoxicity prediction. We further show that internal validation does not guarantee generalizability. In general, safe SiO_2-NPs can be obtained by modifying their surfaces and using low concentrations. Our work provides a strategy for predicting and explaining the toxicity of any type of engineered nanoparticles in real-world practice.

KEYWORDS: literature data mining; machine learning; nanotoxicity; silica nanoparticles; external validation; CatBoost; corona

Decades of nanotoxicological research have generated a significant amount of data in the literature. Literature data mining or meta-analysis has recently gained popularity for revealing relationships hidden in individual studies.[1–8] Unlike the conventional method, which employed a limited dataset to analyze the toxicity of a given type or several types of nanoparticles, using properties such as particle size and concentration[9–11] and omics-based biomarkers,[12] or to predict other outcomes (cell association and adsorption profile),[13,14] literature data mining generates knowledge by combining data from global evidence (aggregate of individual studies), thus expanding the generalizability to a wider range of experimental settings. This approach to developing data-driven models can be useful for environmental and health-risk analyses.[1]

Literature data mining for cellular toxicity has been reported for cadmium-containing quantum dots,[1,2] carbon nanotubes,[3] graphene,[4] micro and nanoplastics,[5] nanoparticles,[6] phytosynthesized silvers,[7] and zinc oxides.[8] These reports presented models for analyzing or predicting nanotoxicity based on their physicochemical properties and experimental settings, using cross-validation or split-sample internal validation to avoid the risk of overlearning the relationships in the data collected. However, if the data collected from the literature contain errors and/or biases, cross-validation or split-sample internal validation becomes biased.[15] Biased validation can also arise from input data or samples that are not representative of the population.[16] Consequently, models validated only internally often lead to misleadingly high predictive performance.[17] Therefore, external validation, using an independently derived dataset, is essential for ensuring generalizability in prediction research.[15–17]

Because nanoparticles adsorb biomolecules present in biological fluids (*e.g.*, serum) to form biomolecular coronas, nanoparticle-corona complexes, and not pristine nanoparticles, interact with biological systems,[18] conceivably, nanoparticle–corona complexes should be considered while building nanoparticle toxicity models. However, none of the existing reports[1–8] externally validate their models or evaluate the toxicological impact of preformed coronas in biological environments, which limits their generalizability in real-world practice. Hence, a cost-effective and rapid method is necessary for reliably developing a prediction model for nanotoxicity.

Amorphous silica nanoparticles (SiO_2-NPs) are used in the manufacture of rubber, paints, cosmetics, biomedicine, and the food additive E551.[19–22] Despite being considered a safety

concern by the Scientific Committee on Consumer Safety (SCCS)[23], SiO_2-NPs are still widely produced and used;[24–26] therefore, their safety deserves the highest priority. *In vitro* cytotoxicity testing has been effectively used to assess SiO_2-NP safety and is the standard used to determine the biocompatibility of commercial medical devices.[27,28] A review of *in vitro* studies reported that smaller SiO_2-NPs tend to induce greater toxicities.[29] Attributes such as concentration, exposure time, surface chemistry, and synthetic pedigrees may also mediate SiO_2-NP toxicity.[24–26] However, despite many *in vitro* toxicological studies, the global causes of SiO_2-NP toxicity remain unclear.[24]

In this study, we propose a method for developing evidence-based prediction models that can distinguish between cytotoxic and noncytotoxic nanoparticles at a given condition based on global evidence. Literature-mined SiO_2-NP cellular toxicity data were used to illustrate the feasibility of this goal. The method employed literature data mining, machine learning, and Shapley Additive exPlanations (SHAP) values[30] with nested cross-validation (nCV)[31] and internal and external validations as proofs of generalizability. To achieve generality and interpretability, we first compiled a highly heterogeneous main dataset of individual studies with various attributes and then built an interpretable prediction model using identified key attributes. The model satisfactorily predicted and explained independent external toxicity data, proving the validity and reliability of the method.

Results and Discussion

Overview of the Method

Figure 1 illustrates the framework for an evidence-based prediction of the toxicity of engineered nanoparticles, with SiO_2-NPs as the test platform and cytotoxicity as the toxicity metric. The input attributes (SiO_2-NP physicochemical properties, experimental settings, and cell types) and binary output responses (cytotoxic or noncytotoxic), *i.e.*, data that closely reflected the actual experiments, were first manually collected from the literature and tabulated. To provide a cost-effective and rapid screening model in risk assessment for biocompatibility evaluation, the cytotoxic response was standardized using the definition of cytotoxicity issued by the International Standard Organization (ISO) in ISO 10993-5, *i.e.*, the cytotoxic effect (positive label) was defined as more than 30% cell-viability reduction.[27,28] All attributes were initially used to train the predictive model (generating an output response from the input attributes), using multiple machine-learning algorithms. SHAP

values were then used to identify the key attributes that contributed to SiO_2-NP toxicity. To demonstrate generalizability, the predictive model had to undergo three critical validations: nCV, internal validation, and external validation. Unlike the optimistically biased estimates from non-nested cross-validation (CV), those from nCV prevent data leakage, using an inner-loop CV nested in an outer CV to select a model (hyperparameter tuning *via* grid search) and an outer CV to evaluate the tuned model.[31]

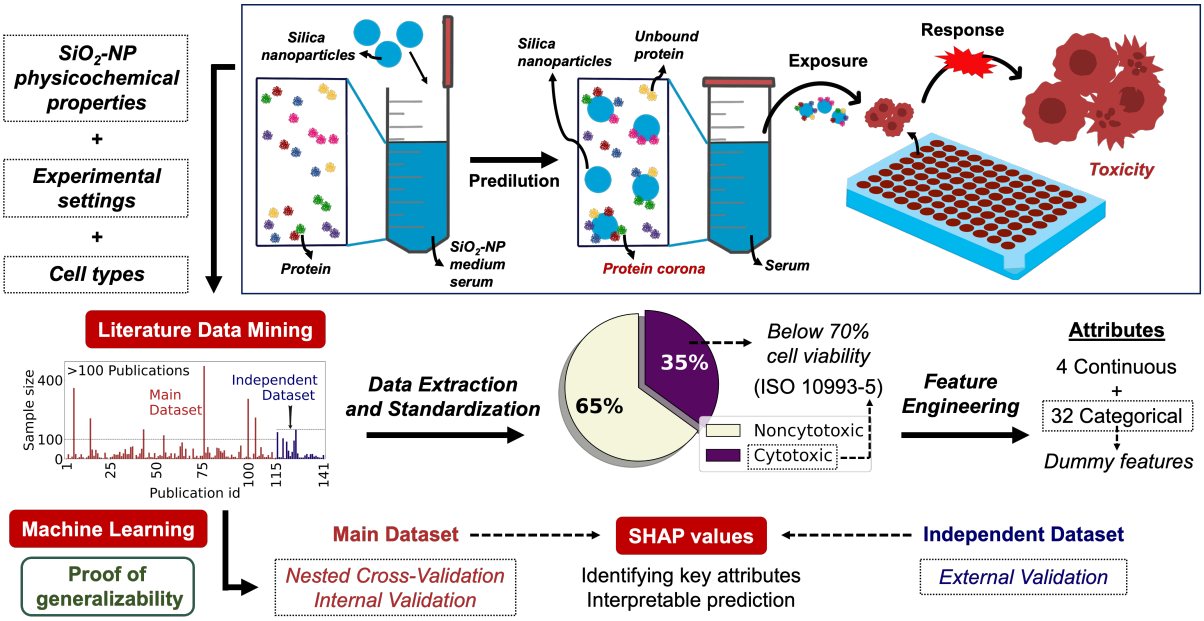

Figure 1. Framework of an evidence-based prediction method. *In vitro* cellular toxicity data were collected from published literature and standardized. Nested cross-validation, internal validation, and external validation were used to prove generalizability.

Literature Data Curation and Nested Cross-validation (nCV)

We obtained cell-viability data for 4124 samples, along with 32 categorical and 4 continuous attributes describing the relevant SiO_2-NP cellular toxicity, from 115 articles published between 2004 and 2016 (Figure 2). Based on the ISO-10993-5 definition, 35% of the 4124 samples were cytotoxic and 65% were noncytotoxic. Table 1 lists the collected attributes. The distribution of the attributes is shown in Supporting Information Figure S1. Compared with the datasets of cadmium-containing quantum dots (3028 samples, 24 attributes)[1,2] and nanoparticles (2986 samples, 15 attributes),[6] our dataset was 36% and 38% larger, respectively, and our attributes were 50% and 140% more diverse, respectively.

Table 1. Attributes of silica nanoparticles

No.	Attributes	Definition
SiO_2-NP Physicochemical Properties		
1	Primary_size	The average size of SiO_2 in the dry state measured by transmission electron microscopy (TEM), scanning electron microscope (SEM), or particle sizer.
2.	Primary_size_verification	The primary size of SiO_2 verified by the individual study, verified elsewhere (cited in previous publication), or not verified (directly used from manufacturer's specifications).
3.	Surface_area	The total area of SiO_2 surface measured by Brunauer–Emmett–Teller (BET) method or calculated by $^6/_{dr}$, where *d* is primary size in mm, *r* is density in g/cc.
4.	Hydrodynamic_size_water	The average hydrodynamic size of SiO_2 measured by dynamic light scattering in water.
5.	Hydrodynamic_size_culture	The average hydrodynamic size of SiO_2 measured by dynamic light scattering in culture medium.
6.	Hydrodynamic_size_serum	The average hydrodynamic size of SiO_2 measured by dynamic light scattering in medium containing serum.
7.	Zeta_potential_water	The electrical potential of SiO_2 at the slipping plane or interface between SiO_2 surface and its water.
8.	Zeta_potential_PBS/HBSS	The electrical potential of SiO_2 at the slipping plane or interface between SiO_2 surface and its phosphate buffered saline (PBS) or Hank's balanced salt solution (HBSS).
9.	Zeta_potential_culture	The electrical potential of SiO_2 at the slipping plane or interface between SiO_2 surface and its culture medium.
10.	Zeta_potential_serum	The electrical potential of SiO_2 at the slipping plane or interface between SiO_2 surface and its medium containing serum.
11.	PDI_water	Polydispersity index (PDI), a measure of broadness of SiO_2 weight distribution in water.
12.	PDI_culture	Polydispersity index (PDI), a measure of broadness of SiO_2 weight distribution in culture medium.
13.	Surface_modification	The SiO_2 surface modifier, *e.g.*, chitosan, carboxyl, and amine.
14.	Surface_charge_water	The electrical charge of SiO_2 present at an interface in water.
15.	Surface_charge_culture	The electrical charge of SiO_2 present at an interface in culture medium.
16.	SiO_2-NP_synthesis	The SiO_2 synthetic pedigrees produced at high (*e.g.*, pyrolytic) or low (colloidal) temperature.
17.	SiO_2-NP_source	The source of SiO_2 obtained from in-house or commercial.
18.	SiO_2-NP_shape	The shape of SiO_2, either sphere or rod.
19.	SiO_2-NP_label	The label of SiO_2 including fluorescein-5-isothiocyanate (FITC), rhodamine, and iodine-125.
Experimental Settings		
20.	Concentration	A measured quantity of SiO_2 in μg/mL for exposure to cells.
21.	Exposure_time	The exposure duration of SiO_2 to cells.
22.	SiO_2-NP_medium_serum	The SiO_2 medium containing different serum concentrations (*e.g.*, serum-free, 10% fetal bovine serum [FBS], and bovine serum albumin [BSA]) for dilution or storage (prior exposure to cells).
23.	Assay_viability	An assay for measuring the cell viability, such as 3-(4,5-dimethylthiazol-2-yl)-2,5-diphenyl-2H-tetrazolium bromide or MTT.
24.	Viability_indicator	Cell viability indicator, *e.g.*, tetrazolium, lactate dehydrogenase (LDH), and adenosine triphosphate (ATP).
25.	Viability_mechanism	Cell viability testing methods including structural cell damage, cell growth, and cellular metabolism.
26.	Interference_testing	The interference of SiO_2 with cell viability assay systems, either performed or not performed by the individual study.
27.	Positive_control	The use of positive control inducer, either included or not included by the individual study.
28.	Positive_control_inducer	A replicate containing all components of a test system and treated with a chemical/particle known to induce a positive response.
29.	Exposure_medium	The culture medium used during SiO_2 exposure to cells.
Cell Types		
30.	Cell_organ	Refers to organ or tissue from which cells originated.
31.	Cell_id	Identifies a specific cell, *e.g.*, A549, RAW 264.7, and HeLa.
32.	Cell_morphology	Refers to morphology of cells, mostly based on american type culture collection (ATCC), *e.g.*, epithelial, endothelial, and fibroblast.
33.	Cell_culture	The culture of cells, either primary cells (isolated from parental tissue) or cell lines (originated from primary cells).
34.	Cell_source	The source of cells including human, mouse, rat, pig, and hamster.
35.	Cell_age	The age of cells including embryonic and nonembryonic.
36.	Cell_disease	The disease stage of cells, either carcinoma or non-carcinoma.

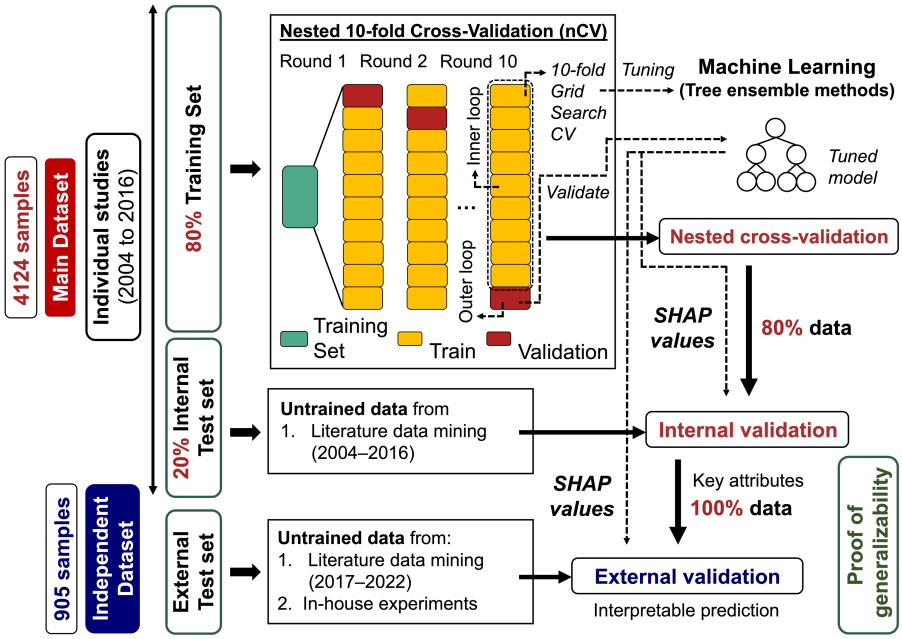

Figure 2. Data preparation: 80% of the main dataset containing all the attributes was trained and cross-validated using 10-fold nCV to develop the predictive model. The remaining 20% was used to internally validate the predictive model and identify the key attributes. Finally, 100% of the main dataset was used to build the final predictive model employing the identified key attributes to predict the independent dataset.

We performed nCV on 80% of the main dataset to obtain an early unbiased estimate of the accuracy of the predictive models (see Methods and Figure 2), and we found that tree-based classifiers exhibited a good fit to the data and outperformed linear, deep neural network (DNN), and nonlinear kernel classifiers, with CatBoost providing the highest nCV accuracy of 91.0±1.5% (Table 2).

Table 2. Prediction-error comparisons: Internal validation (All 36 attributes and 824 samples)

Machine Learning	$nCV_{10\text{-fold}}$	Accuracy	AUC-ROC	Recall	Precision
Linear					
LDA	74.5±2.5%	75.2%	82.6%	56.2%	68.0%
LR	82.3±1.9%	83.4%	89.8%	73.3%	78.4%
Ridge	75.4±2.3%	75.3%	82%	52.7%	70.0%
Nonlinear					
DNN	75.2±1.7%	75.7%	82.7%	61.8%	67.1%
Kernel					
KNN	85.3±1.8%	84.6%	82.5%	75.3%	80.0%
SVM	84.3±1.8%	83.0%	87%	70.5%	79.2%
Tree-based					
DT	87.3±1.8%	85.6%	86.0%	81.5%	78.5%
Extra Trees	86.9±1.8%	85.6%	94.1%	76.7%	81.5%
RF	88.1±1.9%	87.4%	94.5%	79.5%	84.1%
CatBoost	91.0±1.5%	90.4%	96.3%	85.6%	87.1%
GB	90.3±2.0%	89.1%	95.3%	83.6%	85.3%
LightGBM	90.0±1.6%	90.1%	95.8%	84.9%	86.7%
XGBoost	90.2±1.7%	89.9%	95.8%	84.9%	86.4%

Footnotes: LDA, linear discriminant analysis; LR, logistic regression; DNN, deep neural network; KNN, k-nearest neighbors; SVM, support vector machine; DT, decision tree; Extra Trees, extremely

randomized trees; RF, random forest; CatBoost, categorical boosting; GB, gradient boosting; LightGBM, light gradient boosting machine; XGBoost, extreme gradient boosting.

Internal Validation and Attribute Importance

Split-sample internal validation using unbiased representative samples provides an unbiased estimate of the generalization performance of predictive models on unseen data. Table 2 presents the statistical scores of the internal test set (see Methods and Figure 2), with accuracy and area under the receiver operating characteristic curve (AUC-ROC) as the primary evaluation metrics. Tree-based classifiers exhibited satisfactory accuracies of 85.6–90.4% and excellent AUC-ROCs of 94.1–96.3% (except for Decision Tree [DT], with 86.0%), while linear, DNN, and nonlinear kernel classifiers exhibited 75.2–84.6% accuracies and 82–89.8% AUC-ROCs. CatBoost outperformed the other algorithms (accuracy: 90.4%, AUC-ROC: 96.3%, recall: 85.6%, and precision: 87.1%).

We applied attribute importance for attribute selection using SHAP values *via* CatBoost. Based on attribute importance (Figure 3A), we identified the top 13 attributes that provided the optimal predictive accuracy (Figure 3B) and arranged them in the order of importance: *concentration, SiO_2-NP_medium_serum, cell_morphology, cell_organ, primary_size, cell_id, exposure_time, surface_modification, hydrodynamic_size_water, cell_source, assay_viability, surface_area,* and *viability_indicator* (see Table 1 and Supporting Information Figure S1).

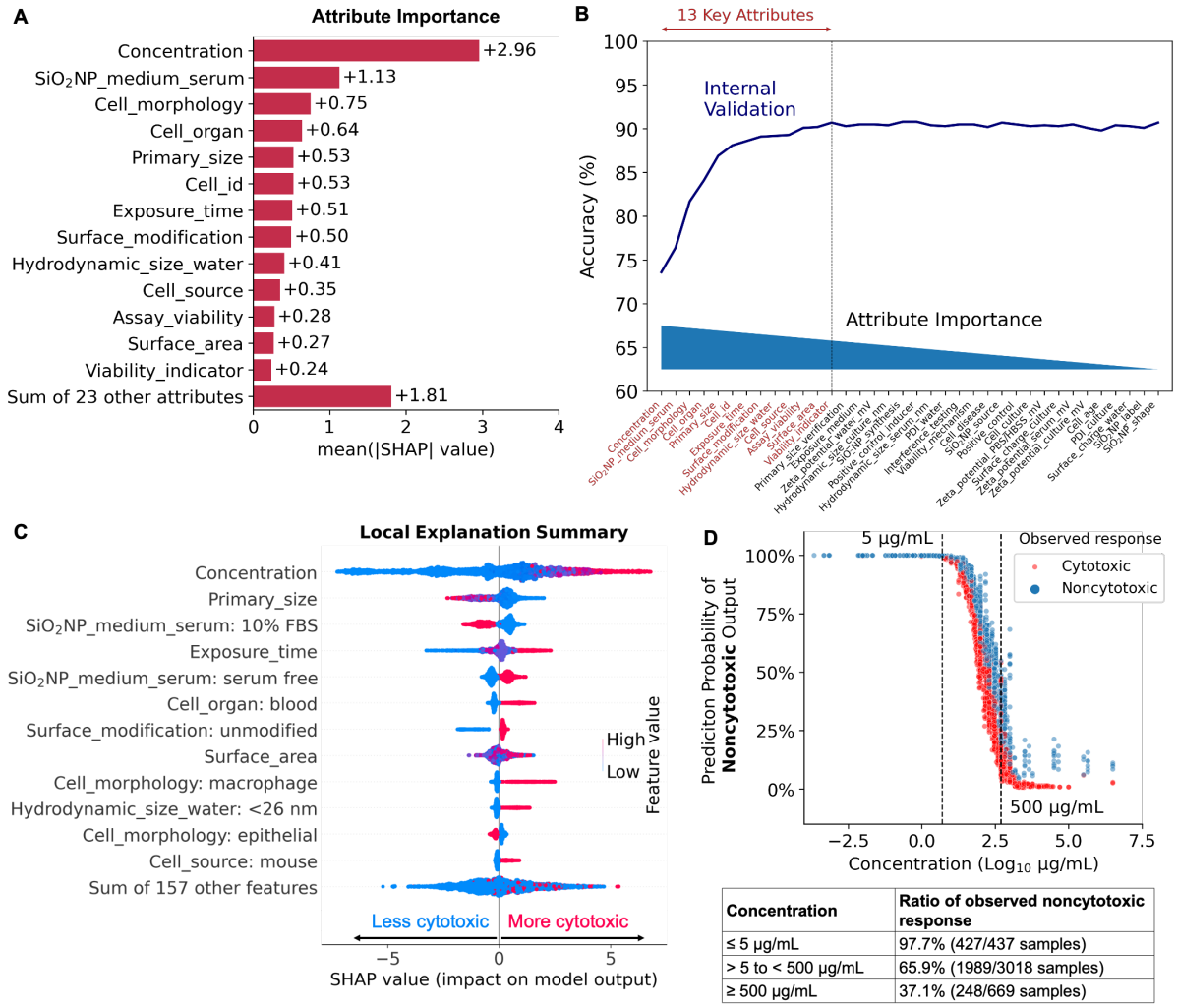

Concentration	Ratio of observed noncytotoxic response
≤ 5 µg/mL	97.7% (427/437 samples)
> 5 to < 500 µg/mL	65.9% (1989/3018 samples)
≥ 500 µg/mL	37.1% (248/669 samples)

Figure 3. Attribute importance for silica nanoparticles, based on CatBoost. (A) Global interpretability for the average absolute SHAP value magnitudes. (B) Predictive accuracy of internal validation with incrementally increasing attributes. (C) Local interpretability, with each dot corresponding to a sample of silica nanoparticle cellular toxicity obtained from 100% of the main dataset. (D) The prediction probability of CatBoost to output a noncytotoxic class at a given condition of concentration attribute alone, using 100% of the main dataset.

We subsequently rebuilt the predictive models using the 80% of the main dataset and the identified key attributes and evaluated their performance. Table 3 presents the statistical scores of nCV and internal validation (the internal test set), using the 13 key attributes. Instead of using all the attributes (Table 2), comparable performance was obtained using only the 13 key attributes, with CatBoost providing the best performance (accuracy: 90.7%, AUC-ROC: 95.9%, recall: 85.6%, precision: 87.7%, and nCV: 90.3±1.9%). Other tree-based classifiers (random forest [RF], gradient boosting [GB], light gradient boosting machine [LightGBM], and extreme gradient boosting [XGBoost]) also exhibited high scores (accuracy >88%, AUC-ROC >94%, recall >81%, precision >85 %, and nCV >88%).

Table 3. Prediction-error comparisons: Internal validation (13 key attributes and 824 samples)

Machine Learning	$nCV_{10\text{-fold}}$	Accuracy	AUC-ROC	Recall	Precision
Linear					
LDA	74.1±2.2%	73.9%	80.4%	48.6%	68.6%
LR	74.7±2.1%	73.3%	80.2%	45.5%	68.6%
Ridge	74.4±2.1%	73.9%	80%	46.9%	69.5%
Nonlinear					
DNN	74.2±2.9%	76.3%	83.7%	67.3%	66.4%
Kernel					
KNN	85.1±1.9%	85.2%	82.8%	74.7%	82.0%
SVM	85.2±1.9%	85.2%	89%	73.3%	82.9%
Tree-based					
DT	86.3±1.5%	87.3%	86.2%	81.2%	82.6%
ET	86.5±2.0%	86.1%	94.1%	77.1%	82.4%
RF	88.1±2.0%	88.8%	94.9%	81.2%	86.5%
CatBoost	90.3±1.9%	90.7%	95.9%	85.6%	87.7%
GB	89.4±2.0%	89.0%	95.1%	83.2%	85.3%
LightGBM	88.5±1.6%	89.1%	95.1%	82.9%	85.8%
XGBoost	89.4±1.5%	89.7%	95.4%	83.9%	86.6%

Footnotes: LDA, linear discriminant analysis; LR, logistic regression; DNN, deep neural network; KNN, k-nearest neighbors; SVM, support vector machine; DT, decision tree; Extra Trees, extremely randomized trees; RF, random forest; CatBoost, categorical boosting; GB, gradient boosting; LightGBM, light gradient boosting machine; XGBoost, extreme gradient boosting.

Finally, we built the final predictive models using 13 key attributes from 100% of the main dataset (4124 samples) and obtained robust nCV accuracy (Table 4). We then analyzed the SHAP-value distribution of the 13 key attributes across the samples. According to the SHAP local explanation summary (Figure 3C), a larger SiO_2-NP primary size, the presence of 10% fetal bovine serum (FBS) in the SiO_2-NP medium (prior exposure to cells), surface-modified SiO_2-NPs, and cells with epithelial morphologies could cause less cytotoxic effects. In contrast, a higher concentration of SiO_2-NPs, a higher exposure time and surface area, a hydrodynamic size less than 26 nm in water, the absence of serum in the SiO_2-NP medium, and the presence of blood cells, macrophage cells, mouse cells, and a tetrazolium viability indicator with an MTT assay (Supporting Information Figure S2) possibly caused a higher cytotoxicity. Supporting Information Figure S2 presents a complete summary of the local explanation. Although concentration was identified as a leading attribute determining SiO_2-NP toxicity, SiO_2-NPs with concentrations >5 μg/mL alone could not be used for an accurate prediction, as shown in Figure 3D. Notably, 97.7% of SiO_2-NPs with concentrations ≤5 μg/mL were associated with noncytotoxicity. No obvious thresholds were identified for other continuous attributes (Supporting Information Figure S3). Additionally, we identified a single DT with an nCV accuracy of 73.4±1.9% (Supporting Information Figure S4) for a simple guidance on

SiO_2-NP toxicity; however, to maximize the predictive power of our final model, we recommend using all 13 key attributes when using our model *via* Google Colab.

Table 4. Prediction-error comparisons: External validation (13 key attributes and 905 samples)

Machine Learning	$nCV_{10\text{-fold}}$	Accuracy	AUC-ROC	Recall	Precision	True Positive	False Positive	True Negative	False Negative
Linear									
LDA	73.6±2.4%	65.2%	70.2%	64.4%	38.2%	145	235	445	80
LR	74.4±2.5%	64.4%	64.1%	57.8%	36.4%	130	227	453	95
Ridge	74.3±1.8%	65.3%	70%	63.6%	38.1%	143	232	448	82
Nonlinear									
DNN	75.3±2.1%	65.5%	68.1%	52.4%	36.3%	118	205	474	107
Kernel									
KNN	86.5±1.4%	74.0%	71.7%	67.1%	48.4%	151	161	519	74
SVM	86.3±2.1%	75.9%	46%	3.1%	100.0%	7	0	680	218
Tree-based									
DT	87.7±1.6%	67.4%	59.7%	44.0%	36.9%	99	169	511	126
Extra Trees	87.5±1.8%	82.3%	88.4%	57.8%	66.7%	130	65	615	95
RF	88.7±1.6%	85.1%	91.4%	48.4%	85.2%	109	19	661	116
CatBoost	90.5±1.6%	88.1%	92.0%	72.4%	78.0%	163	46	634	62
GB	89.8±1.4%	87.8%	90.2%	66.2%	81.4%	149	34	646	76
LightGBM	89.3±1.3%	82.0%	88.1%	67.6%	62.8%	152	90	590	73
XGBoost	89.6±1.4%	84.5%	88.4%	61.3%	72.3%	138	53	627	87

Footnotes: A model that always generates a noncytotoxic class affords an accuracy of 75.1% (680/905). LDA, linear discriminant analysis; LR, logistic regression; DNN, deep neural network; KNN, k-nearest neighbors; SVM, support vector machine; DT, decision tree; Extra Trees, extremely randomized trees; RF, random forest; CatBoost, categorical boosting; GB, gradient boosting; LightGBM, light gradient boosting machine; XGBoost, extreme gradient boosting.

External Validation

An independent dataset (905 samples) was generated separately from the main dataset. Thus, predicting and explaining the independent dataset made this task more challenging, valuable, and relevant for real-world practice. The external validation results (Table 4) demonstrated that CatBoost allowed for a satisfactory generality and delivered the highest performance (accuracy: 88.1%, AUC-ROC: 92.0%, recall: 72.4%, and precision: 78.0%), followed by GB, RF, and XGBoost (accuracies >84% and AUC-ROCs >88%). However, RF showed the worst recall (48.4%) among the tree-ensemble classifiers; therefore, unlike the boosting algorithms (CatBoost, GB, XGBoost, and LightGBM) with >61% recall, RF was deemed unsuitable for identifying all positive samples. With 64.4–75.9% accuracies, the linear, DNN, nonlinear kernel, and DT classifiers were difficult to fit to the independent dataset. The support vector machine (SVM) only predicted the majority noncytotoxic class (true positives: 7, false positives: 0, true negatives: 680, and false negatives: 218) and exhibited the worst AUC-ROC and recall of 46% and 3.1%, respectively, indicating that

it misclassified the independent cytotoxicity data 54% of the time and failed to identify all positive samples.

To confirm and elucidate the influence of serum in predicting SiO_2-NP toxicity, we rebuilt the predictive models using 12 key attributes by excluding the *SiO_2-NP_medium_serum* attribute. In general, the results indicated substantially worse performance (CatBoost: accuracy, 80.7%; AUC-ROC, 84.4%; recall, 53.3%; precision, 63.2%; and nCV, 88.7±1.3%), underscoring the importance of nanoparticle–corona formation in biological environments containing various serum concentrations for a highly accurate prediction (Supporting Information Table S1). Meanwhile, Supporting Information Figure S5 shows that the predictive models generally exhibited a lower performance when all 36 attributes were used, indicating that attribute selection was essential to preventing overfitting while dealing with a truly independent test set.

External validation is crucial for the real-world implementation of a highly accurate generalization.[15–17] The CatBoost model consistently demonstrated satisfactory performance for both internal validation (accuracy: 90.7%, AUC-ROC: 95.9%, recall: 85.6%, and precision: 87.7%; nCV: 90.3±1.9%) and external validation (accuracy: 88.1%, AUC-ROC: 92.0%, recall: 72.4%, and precision: 78.0%; nCV: 90.5±1.6%). Thus, CatBoost provided a more promising algorithm for the generalizability of nanotoxicity than the previously used RF or DT.[1,3–8] In contrast, DT and kernel classifiers that performed well on internal validation showed unexpectedly poor performance for external validation, highlighting its pivotal role.

Complex Relationships of SiO_2-NP Attributes with Cellular Toxicity

We selected CatBoost to represent the prediction results of external validation. We then performed hierarchical clustering and grouped the independent datasets by their explanation similarity (SHAP values) for heterogeneity visualization (Figure 4A). Supporting Information Figures S6-S7 show the prediction errors for 905 samples (55 sets of experiments). Figures 4B and 4C present two of the 55 sets of experiments as representative samples. Decision plots of the correctly classified and misclassified samples are shown in Supporting Information Figure S8. To ensure the applicability of the model in real-world practice, we quantitatively elucidated the CatBoost process that generates the output cytotoxicity response from the input key attributes using SHAP values. The

rational decision-making shown in Figures 4D–G and Supporting Information Rationality illustrates the complex attribute relationships of a potential SiO_2-NP hazard while inducing toxicity in cellular machinery. The underlying mechanisms related to concentration, time, size, surface, cell, and serum attributes could be triggered by the cellular uptake of SiO_2-NPs.[32–36] The role of serum attribute in the prediction of SiO_2-NP toxicity is clear; preformed coronas in the presence of the serum may mitigate SiO_2-NP toxicity. Corona formation alters the ability of cell receptors to recognize SiO_2-NPs and, by lowering the SiO_2-NP surface energy, prevents silanols [≡Si–OH and =Si$(OH)_2$] from interacting efficiently with the biomembranes, thereby reducing the SiO_2-NP uptake efficiency.[34–36] However, the absence of the serum can cause more cytotoxic effects, because the surface silanols of the SiO_2-NPs can then directly interact with and disrupt the cellular membranes *via* hydrogen bonding and electrostatic interactions. In fact, a specific surface-silanol pattern, referred to as “nearly free silanol”, promotes membranolysis by interacting with phosphatidylcholine (a biomembrane lipid), regardless of silica crystallinity,[37] supporting that surface modification can reduce SiO_2-NP toxicity.

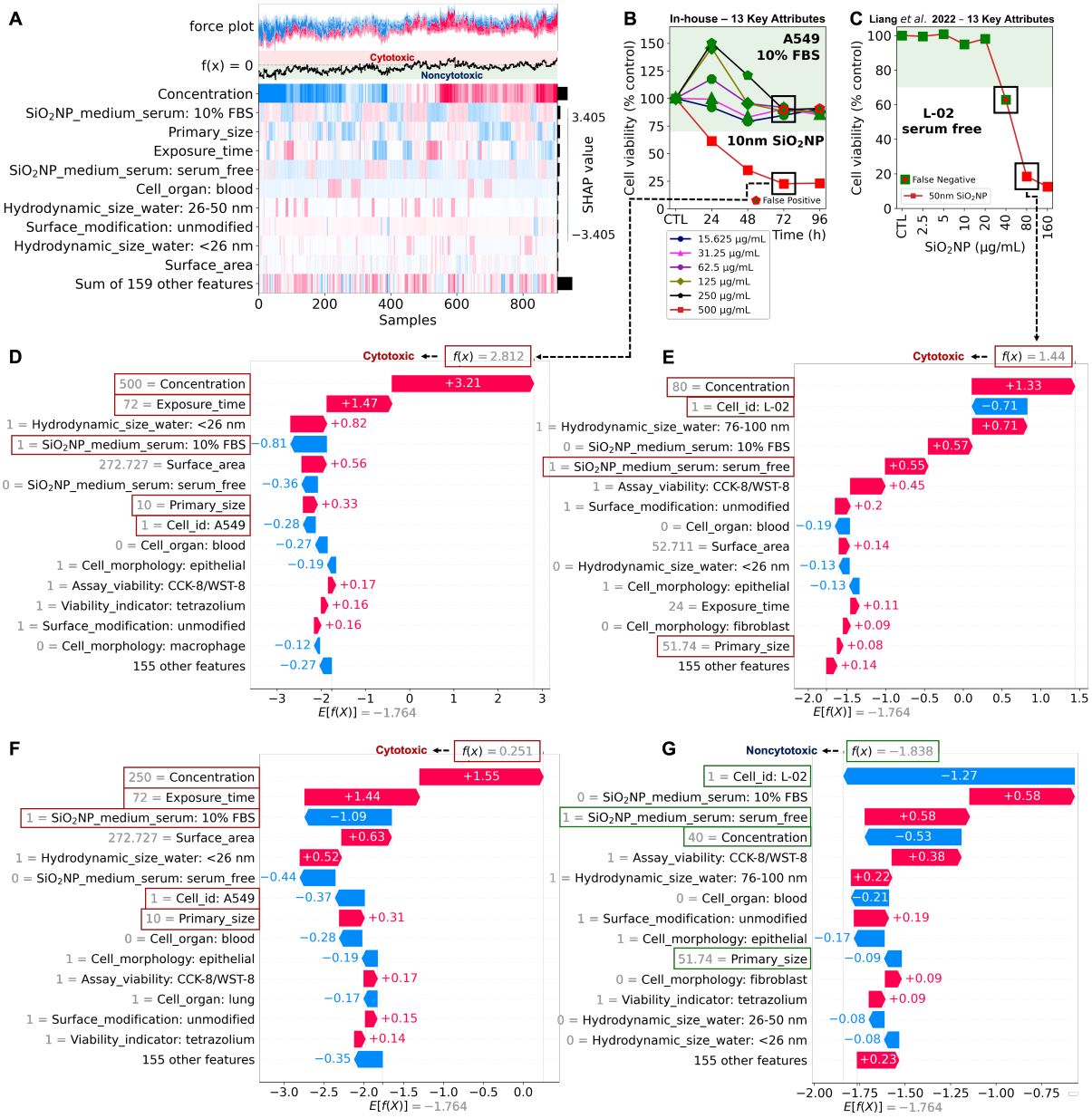

Figure 4. Prediction errors generated by the CatBoost model upon external validation. (A) SHAP heatmap plot. Samples with similar SHAP-value-based explanations were grouped together *via* hierarchical clustering. Increasing and decreasing cytotoxicity by attribute value are indicated in red and blue, respectively. The force plot at the top corresponds to the ratios of attribute values with a negative magnitude (blue) to those with a positive magnitude (red); f(x) = 0 corresponds to the predicted cytotoxicity. Samples predicted to be cytotoxic and noncytotoxic are shown in the red and green regions, respectively. (B and C) Prediction errors of each sample from two of the 55 sets of experiments. Red and green markers indicate cytotoxicity and noncytotoxicity, respectively. Correctly classified samples have either a green or red marker, whereas misclassified samples have markers that are a combination of both colors. (D and E) Two examples of correctly classified samples. The positive values of f(x) = 2.812 and f(x) = 1.44 correspond to the cytotoxic class and were generated from the sum of the base value (–1.764) and the additive contributions of each attribute value (3.21 + 1.47 + …. – 0.27 in f(x) = 2.812 and 1.33 – 0.71 + …. + 0.14 in f(x) = 1.44). They explain which attribute value corresponded to the predicted cytotoxicity values of 2.812 and 1.44 from the base value; for example, in f(x) = 2.812, *concentration: 500 μg/mL* increased the base value by 3.21, whereas *SiO_2-NP_medium_serum: 10%_FBS* decreased it by 0.81. The base value was the average cytotoxicity value of the entire main dataset. (F and G) Two examples of misclassified samples. The positive and negative values of f(x) = 0.251 and f(x) = –1.838 correspond to the cytotoxic and noncytotoxic class, respectively.

Despite evidence from various individual studies showing that biomolecular corona fingerprints can predict biological behaviors of nanoparticles,[12,13,14] previous literature data mining reports[1–8] failed to recognize that nanoparticles rapidly form protein coronas in less than 30 s, once in contact with biological fluids.[38] Thus, nanoparticle–corona complexes interact with cells,[18,34–36] not pristine nanoparticles, in the presence of serum. We hypothesize that incorporating the biological medium attribute (*e.g.*, *SiO_2-NP_medium_serum* attribute) is a prerequisite for accurately predicting nanotoxicity. This is supported by the observation that not only is the *SiO_2-NP_medium_serum* attribute closely correlated to SiO_2-NP toxicity, but its omission also causes a substantial and general drop in predictive performance. These observations warrant a reconsideration of nanotoxicity models, as developing predictive toxicity models for engineered nanoparticles without considering preformed coronas in biological environments has limited success.

Evidence shows that SiO_2-NPs produced at high temperatures (pyrolytic) are more toxic than those produced at low temperatures (colloidal).[24] However, we could not identify the *SiO_2-NP_synthesis* attribute as a key attribute, possibly because only one study directly compared pyrolytic and colloidal SiO_2-NPs with different synthetic pedigrees under identical conditions.[39] More in-depth investigations are required to confirm the influence of synthetic pedigrees, including variations in size, surface, cell, assay, and biological media, on SiO_2-NP toxicity. This study did not include all possible individual studies. Future research may expand on this study by including more studies, to develop a more powerful and generalizable predictive model for SiO_2-NP toxicity. Although we contemplated utilizing the target cellular dose or the number of particles as the concentration attribute, we encountered a limited amount of data in the literature that provided such information. Consequently, we used the administered concentration as the concentration attribute in our models, which enabled a larger sample size and better generalizability. However, it is crucial to acknowledge that actual cellular dose or number of particles may offer greater accuracy in predicting cellular toxicity. Therefore, future research may consider incorporating cellular dose or number of particles data, if obtainable. Additionally, the physicochemical properties of SiO_2-NPs could be characterized more comprehensively, as many unmeasured (*not_determined*) values were found in the collected data (Supporting Information Figure S1).

Despite efforts to adhere to ISO 10993-5 in assay selection, the MTT assay might not be entirely reliable for predicting the toxicity of some nanoparticles, including SiO_2-NPs. This might limit the accuracy of our predictive models, underscoring the importance of utilizing multiple assays to fully assess nanoparticle toxicity. It should be noted that our current *in vitro* findings cannot be directly extrapolated to *in vivo* outcomes. While we presented an extended framework for *in vivo* studies in Supporting Information Figure S9, we recognize the challenge of establishing *in vitro-in vivo* correlation (IVIVC) and the need for future prediction research in this area. Different nanoparticles show different toxicity profiles, and to define the scope of a predictive model appropriately, a specific type of nanoparticles should be used while building the model. Finally, future studies should avoid exaggerated claims of accurate predictions of nanotoxicity spectra while using limited datasets without external validation.

Conclusions

Distinguishing between cytotoxic and noncytotoxic engineered nanoparticles is important for nanosafety. A derived CatBoost model revealed key SiO_2-NP attributes for predicting toxicity: *concentration, SiO_2-NP_medium_serum, cell_morphology, cell_organ, primary_size, cell_id, exposure_time, surface_modification, hydrodynamic_size_water, cell_source, assay_viability, surface_area,* and *viability_indicator*. It established an evidence-based prediction method capable of predicting SiO_2-NP toxicity, using the aforementioned key attributes derived from global evidence. This was achieved *via* extensive literature data mining, covering 115 publications, and the generation of the largest dataset to date, containing 36 of the most diverse attributes of SiO_2-NP cellular toxicity and 4124 samples, in addition to an independent dataset containing 905 samples.

Developing a reliable and robust general predictive model is a challenge for nanotoxicological research. A computationally attractive means of addressing this task is to aggregate information provided by global evidence, so that the generalizability can be extended to inter-laboratory settings. Despite a considerable interest therein, there is no proven method to reliably predict nanotoxicity. Herein, we developed an evidence-based prediction method capable of distinguishing between cytotoxic and noncytotoxic nanoparticles at a given condition, based on

global evidence. We used SiO_2-NPs to illustrate the reliable development of predictive models from scratch and identified the key attributes (concentration, serum, cell, size, time, surface, and assay) contributing to SiO_2-NP toxicity. In general, safe SiO_2-NPs can be obtained by modifying their surfaces (*e.g.*, carboxyl and chitosan) and using low concentrations (*e.g.*, ≤5 μg/mL). We demonstrated the application of CatBoost[40] (unbiased boosting) as an effective tool for nanotoxicity prediction. To ensure the applicability of the CatBoost model in real-world practice, we elucidated its interpretability while generating cytotoxicity responses using the key attributes and highlighted the cruciality of external validation. Certain models that performed well on internal validation performed poorly on the independent dataset, indicating that internal validation does not guarantee generalizability. We further showed that the incorporation of biological media attributes, such as serum, can predict nanotoxicity accurately, owing to the formation of nanoparticle–corona complexes. Through a comprehensive analysis of global evidence, we incorporated generalized key attributes that may not be readily apparent in individual studies into the CatBoost model. This model can be a valuable tool for researchers to design experiments to predict and explain the potential toxicity of SiO_2-NPs under specific conditions and guide the development of safer SiO_2-NPs.

Regarding the future prospects of the method developed in this study, in a broader context, the method of integrating literature data mining, machine learning, and SHAP values with nCV and internal and external validations as proofs of generalizability has the potential to provide a generic and open platform to examine any type of engineered nanoparticles, to predict not only their toxicity but also other biological outcomes in more complex systems, such as changes in nanoparticle uptake into cells owing to differences in the types of biomolecules forming the corona and absorption, distribution, metabolism, and excretion (ADME) processes (Supporting Information Figure S9). Consequently, this study could contribute to the design and application of safe nanoparticles as biomaterials and provide guidance for reliable and explainable predictions in the field of nanoinformatics.

Methods

Literature Data Mining

Two published review papers on SiO_2-NP toxicity were used for the literature data assessment: the Napierska *et al.* review[26] and the Murugadoss *et al.* review,[25] which covered studies published until 2010 and 2016, respectively. The literature was chosen based on population, intervention, comparison, outcomes, and study design or the PICOS framework[41] of evidence-based medicine to ensure homogeneity and reliability, wherein (1) the population comprised human or mammalian cells; (2) the intervention and comparison were amorphous non-mesoporous SiO_2-NPs vs. negative control, with reported concentration, exposure time, and primary size ≤1000 nm; (3) the outcome was cytotoxicity (percentage of cell viability); and (4) the study design was an *in vitro* toxicological study. The exclusion criteria included non-mammalian or co-cultured cells, crystalline or mesoporous SiO_2-NPs, abstract articles, and other non-relevant studies. In these two reviews, 61 studies met our inclusion criteria; therefore, their reference lists were reviewed for further potential literature, and 54 additional eligible studies were identified. In total, 115 studies were included.

The relevant SiO_2-NP attributes and cell-viability data were carefully extracted to generate 4124 samples and 36 attributes. The mean cell viability was extracted from either the text or graphs using WebPlotDigitizer[42] and converted to "1" (<70% cell viability, cytotoxic) and "0" (≥70% cell viability, noncytotoxic) labels. To facilitate the rapid screening of SiO_2-NPs for cellular toxicity without cumbersome experiments, the administered concentration (a measured quantity of SiO_2 in μg/mL for exposure to cells) was used as the concentration attribute. Unless otherwise reported, the surface area (m^2/g) was calculated (surface area = $^{6}/_{dr}$, where *d* is primary size in mm, *r* is density in g/cc). Owing to missing data in the literature, hydrodynamic size, zeta potential, and polydispersity index (PDI) were presented as ranges (categorical attributes). For example, if the hydrodynamic size in water is 18.3 nm, then it will be assigned as "*Hydrodynamic_size_water: <26 nm*," which served as a feature. The missing value in the hydrodynamic size attribute is presented as the value *not_determined*, which served as a feature input for the predictive models. For each categorical attribute, a dummy feature (binary vector) was created and one of the dummy features was removed to prevent a dummy-variable trap (Supporting Information Table S2). A feature is a specific value of an attribute, for example *SiO_2-NP_medium_serum* is an attribute; "*SiO_2-NP_medium_serum: serum_free*" is a feature of the *SiO_2-NP_medium_serum* attribute. Feature

scaling was performed using Min-Max normalization for DNN classifier and z-score normalization for linear and nonlinear-kernel classifiers.

Machine Learning

Thirteen well-established machine-learning algorithms were used (1) linear discriminant analysis (LDA), (2) logistic regression (LR), (3) ridge classifier, (4) DNN, (5) k-nearest neighbors (KNN), (6) SVM, (7) DT, (8) CatBoost, (9) extremely randomized trees (extra trees), (10) GB, (11) LightGBM, (12) RF, and (13) XGBoost. Algorithms 1–3 are linear; 4 is nonlinear; 5 and 6 are nonlinear kernels; and 7–13 are nonlinear tree-based classifiers. A fixed random_state of 2022 was used whenever possible during model development. Machine-learning algorithms were implemented using the scikit-learn (version 1.0.2), tensorflow (version 2.10.0), CatBoost (version 1.0.4), LightGBM (version 3.3.2), and XGBoost (version 1.5.1) packages in Python 3.10.

The entire main dataset (containing 4124 samples) was first shuffled and then split into training (80%) and internal test (20%) sets by applying random stratified sampling (Figure 2). Binary classification predictive models were initially built using 80% of the main dataset, which contained all the attributes, using the 13 machine-learning algorithms. The predictive models were cross-validated using 10-fold nCV, and the data were split into 10 parts in a stratified manner. One part was used as the validation set and the remaining as the training set. The training set was exhaustively tuned to obtain the optimal hyperparameters using 10-fold GridSearchCV in scikit-learn within specific ranges (Supporting Information Tables S3 and S4). The best grid search model was then fitted to the training set, and the predictive accuracy for the validation set was calculated. This process was repeated for each of the 10 parts, and 10 predictive-accuracy values were obtained and averaged as the nCV accuracy.

Internal validation was performed for each algorithm using 20% of the main dataset as the internal test set, which was entirely independent of the building or fine-tuning of the predictive models. The optimal hyperparameters of each algorithm were updated by applying 10-fold GridSearchCV to the training set, and the best model was used to predict the internal test set. The SHAP values were then applied to the training set to uncover the key attributes. The final predictive models were built using 100% of the main dataset and the identified key attributes, and the optimal

hyperparameters of each algorithm were updated by applying 10-fold GridSearchCV to the entire shuffled main dataset. The nCV accuracy for the entire main dataset was also calculated. The optimal hyperparameters were tentative, depending on the input data for the grid search (Supporting Information Tables S3 and S4).

The evaluation metrics were based on accuracy ($1 - \frac{TP + TN}{TP + FP + TN + FN}$), AUC-ROC (area under the curve of the true-positive rate or recall $[\frac{TP}{TP + FN}]$ vs. false-positive rate $[\frac{FP}{FP + TN}]$), recall, and precision $\left(\frac{TP}{TP + FP}\right)$, where TP, TN, FP, and FN represent true positive, true negative, false positive, and false negative, respectively.

External Validation

The final predictive models were used to predict the independent datasets derived from external studies published between 2017 and 2022.[32,43,52–61,44,62–66,45–51] Specifically, Gong *et al*. (2017)[43] exposed HaCaT cells to 15-nm SiO_2-NPs for 24 h (nine samples). Similarly, Liu *et al*. (2017)[44] subjected A549 cells to 15-nm SiO_2-NPs over a period of 24 h (eight samples), whereas Nishijima *et al.* (2017)[45] put 10–1000-nm SiO_2-NPs in contact with THP-1 cells for 6–24 h (105 samples). THP-1 cells were exposed to 50-nm SiO_2-NPs for 22 h (four samples) by Premshekharan *et al.* (2017).[46] Meanwhile, Vicente *et al.* (2017)[47] subjected K17 and HDF cells to SiO_2-NPs with diameters of 20–500-nm for 24 h (88 samples). Kusaczuk *et al.* (2018)[48] examined the effects of exposing 7–20-nm SiO_2-NPs to LN229 cells for 24 and 48 h (42 samples), while Zang *et al.* (2018)[49] separately exposed A549 cells to 20- and 100-nm SiO_2-NPs for 24 h (14 samples). In another study, Du *et al.* (2019)[50] subjected N9, bEnd.3, and HT-22 cells to 50–300-nm SiO_2-NPs for a period of 24 h (36 samples). Similarly, the effects on HEK293 and hippocampal cells when exposed to SiO_2-NPs of various diameters (10–400-nm) for various times (0.08–24 h) were investigated by Kamikubo *et al.* (2019)[51] (93 samples). Similarly, Kim *et al.* (2019)[32] exposed HepG2, A549, and SW480 cells to 20–50-nm SiO_2-NPs for 0.5–24 h (148 samples). Lee *et al.* (2019)[52] subjected HUVEC cells to 20–50-nm SiO_2-NPs for 24 h (28 samples), whereas Ren *et al.* (2019)[53] examined the effects of 57.66-nm SiO_2-NPs on GC-2spd cells over a period of 24 h (seven samples). Crucho *et al.* (2020)[54] exposed HeLa cells to 35-nm SiO_2-NPs for 24 h (seven samples),

while Liu *et al.* (2020)[55] placed BEAS-2B cells in contact with 15-nm SiO_2-NPs for 12 h (seven samples). Meanwhile, A549 cells were exposed to 25-nm SiO_2-NPs for 24–72 h (18 samples) by Nazarparvar-Noshadi *et al.* (2020).[56] Tada-Oikawa *et al.* (2020)[57] subjected Caco-2 cells with 30-nm SiO_2-NPs for 24 h (25 samples), and Wang *et al.* (2020)[58] observed the effects of 16.75-nm SiO_2-NPs on BEAS-2B cells over periods of 24 and 48 h (ten samples). Similarly, Cui *et al.* (2021)[59] exposed H9c2 cells to 60-nm SiO_2-NPs for 6–48 h (24 samples). The effects of exposing SH-SY5Y cells to 63-nm SiO_2-NPs were examined for periods of 3–24 h (25 samples) by Hou *et al.* (2021),[60] while the influence of 16–51-nm SiO_2-NPs on NRK cells for 24 h (12 samples) was investigated by Ruan *et al.* (2021).[61] More recently, Hou *et al.* (2022)[62] exposed BV2 cells to 48.53-nm SiO_2-NPs for 3–24 h (16 samples), while Kim *et al.* (2022)[63] subjected HepG2 cells to 20-nm SiO_2-NPs for a period of 24 h (ten samples). Similarly, Liang *et al.* (2022)[64] observed the effects of 50-nm SiO_2-NPs on L-02 cells for 24 h (seven samples). Finally, Ma *et al.* (2022)[65] exposed BEAS-2B cells to 51.58-nm SiO_2-NPs for 24 h (six samples), and Zhang *et al.* (2022)[66] subjected R28 cells to 15- and 50-nm SiO_2-NPs for periods of 12 and 24 h (20 samples).

Moreover, to verify the final predictive models, we included in-house experiments, which were performed by independent researchers using SiO_2-NPs with primary sizes of 10-, 30-, 50-, 70-, 100-, 300-, and 1000-nm (136 samples). SiO_2-NPs were obtained from Micromod Partikeltechnologie (Rostock, Warnemünde, Germany). The hydrodynamic sizes and zeta potentials of the SiO_2-NPs were measured using a Zetasizer Nano-ZS (Malvern Instruments Ltd.). The hydrodynamic sizes of the 10-, 50-, and 100-nm SiO_2-NPs in water were 18.3, 48.4, and 99.8 nm, respectively; their zeta potentials were –15.6, –17.3, and –22.3 mV, respectively, and their primary sizes were as indicated by the manufacturer. The hydrodynamic sizes and zeta potentials of the 30-, 70-, 300-, and 1000-nm SiO_2-NPs were previously published.[67,68] Experimental details on the exposure of A549, SH-SY5Y, TM4, BeWo, and RAW 264.7 cell lines to SiO_2-NPs are provided in Supporting Information Table S5.

Shapley Additive exPlanations (SHAP)

Attribute importance was determined based on the global feature importance defined by the SHAP values:[30,69]

$\phi_i = \frac{1}{|F|!}\sum_{S\subseteq F\setminus\{i\}}|S|!\,(|F|-|S|-1)!\,[f_{S\cup\{i\}}(x_{S\cup\{i\}}) - f_S(x_S)]$, where $F, S, x_S, f_{S\cup\{i\}}$, and f_S represent the set of all features, a subset of F, the values of the input features in the set S, a trained model with that feature present, and a trained model with that feature withheld, respectively. The SHAP value ϕ_i of the feature i was generated by averaging the marginal contributions of all the permutations of a feature set. A higher mean absolute SHAP value indicated a more predictive feature. In this study, features with positive SHAP values drove the output of the model towards cytotoxicity, and vice versa, thus explaining the rationality of decision-making in prediction.

Data availability

All relevant data are available from the authors upon reasonable request and/or are included in the article and Supporting Information.

Code availability

The code to run the final model is available at https://github.com/martinj-phs/nanosilica.

Competing interests

The authors declare no competing interests.

Supporting Information

- Silica nanoparticles with 32 categorical (heatmap visualization) and 4 continuous (distribution plot visualization) attributes (Figure S1); Complete Local Interpretability by CatBoost Model (Main Dataset: 4124 samples) (Figure S2); Prediction Probability of Noncytotoxity by CatBoost Model (Main Dataset: 4124 samples) (Figure S3); Decision Tree (Main Dataset: 4124 samples) (Figure S4); Predictive Accuracy of External Validation with Incrementally Added Attributes (Figure S5); Prediction Errors of CatBoost Model for Eight Sets of In-house Experiments (136 Samples) (Figure S6); Prediction Errors of CatBoost Model for 47 Sets of Experiments (769 Samples) (Figure S7); Decision Plots of Independent Dataset by CatBoost Model (905 samples) (Figure S8); Extended Framework of an Evidence-Based Prediction Method (*In Vivo* Studies) (Figure S9); Prediction-Error Comparisons: External Validation (12 Key Attributes and 905

samples) (Table S1); List of Removed Dummy Features (Table S2); Hyperparameter Settings for 12 Machine Learning Algorithms for Internal Validation (80% Main Dataset) (Table S3); Hyperparameter Settings for 12 Machine Learning Algorithms for External Validation (100% Main Dataset) (Table S4); Cell Viability Assay (Table S5)

- Rationality of Decision-Making (Independent Dataset: 905 Samples) (Supporting Information Rationality)
- Nanosilica Dataset
- Final Model Code

AUTHOR INFORMATION

Corresponding Authors

Martin

Graduate School of Pharmaceutical Sciences, Osaka University

1-6 Yamadaoka, Suita City, Osaka 565-0871, Japan

Email: martinj.phs@gmail.com, martin@phs.osaka-u.ac.jp

Kenji Mizuguchi

Institute for Protein Research, Osaka University

3-2 Yamadaoka, Suita City, Osaka 565-0871, Japan

Phone No: +81 6-6105-6961

Fax No: +81 6-6105-6962

Email: kenji@protein.osaka-u.ac.jp

Contributions

M. and K.M. conceived and designed the experiments. M. performed the experiments. M., R.W., K.Hashimoto, and K.M. analyzed the data. M., R.W., K.Higashisaka, Y.H., Y.T., and K.M. contributed materials/analysis tools. M., R.W., K.Hashimoto, K.Higashisaka, Y.H., Y.T., and K.M. wrote the paper.

References

(1) Oh, E.; Liu, R.; Nel, A.; Gemill, K. B.; Bilal, M.; Cohen, Y.; Medintz, I. L. Meta-Analysis of Cellular Toxicity for Cadmium-Containing Quantum Dots. *Nat. Nanotechnol.* **2016**, *11*, 479–486. https://doi.org/10.1038/nnano.2015.338.

(2) Bilal, M.; Oh, E.; Liu, R.; Breger, J. C.; Medintz, I. L.; Cohen, Y. Bayesian Network Resource for Meta-Analysis: Cellular Toxicity of Quantum Dots. *Small* **2019**, *15*, e1900510. https://doi.org/10.1002/smll.201900510.

(3) Gernand, J. M.; Casman, E. A. A Meta-Analysis of Carbon Nanotube Pulmonary Toxicity Studies-How Physical Dimensions and Impurities Affect the Toxicity of Carbon Nanotubes. *Risk Anal.* **2014**, *34*, 583–597. https://doi.org/10.1111/risa.12109.

(4) Ma, Y.; Wang, J.; Wu, J.; Tong, C.; Zhang, T. Meta-Analysis of Cellular Toxicity for Graphene via Data-Mining the Literature and Machine Learning. *Sci. Total Environ.* **2021**, *793*, 148532. https://doi.org/10.1016/j.scitotenv.2021.148532.

(5) Xu, J.; Lin, X.; Gowen, A. A. Combining Machine Learning with Meta-Analysis for Predicting Cytotoxicity of Micro- and Nanoplastics. *J. Hazard. Mater. Adv.* **2022**, 100175. https://doi.org/10.1016/j.hazadv.2022.100175.

(6) Labouta, H. I.; Asgarian, N.; Rinker, K.; Cramb, D. T. Meta-Analysis of Nanoparticle Cytotoxicity via Data-Mining the Literature. *ACS Nano* **2019**, *13*, 1583–1594. https://doi.org/10.1021/acsnano.8b07562.

(7) Liu, L.; Zhang, Z.; Cao, L.; Xiong, Z.; Tang, Y.; Pan, Y. Cytotoxicity of Phytosynthesized Silver Nanoparticles: A Meta-Analysis by Machine Learning Algorithms. *Sustain. Chem. Pharm.* **2021**, *21*, 100425. https://doi.org/10.1016/j.scp.2021.100425.

(8) Kad, A.; Pundir, A.; Arya, S. K.; Puri, S.; Khatri, M. Meta-Analysis of in-Vitro Cytotoxicity Evaluation Studies of Zinc Oxide Nanoparticles: Paving Way for Safer Innovations. *Toxicol. Vitr.* **2022**, *83*, 105418. https://doi.org/10.1016/j.tiv.2022.105418.

(9) Puzyn, T.; Rasulev, B.; Gajewicz, A.; Hu, X.; Dasari, T. P.; Michalkova, A.; Hwang, H. M.; Toropov, A.; Leszczynska, D.; Leszczynski, J. Using Nano-QSAR to Predict the Cytotoxicity of Metal Oxide Nanoparticles. *Nat. Nanotechnol.* **2011**, *6*, 175–178. https://doi.org/10.1038/nnano.2011.10.

(10) Manganelli, S.; Leone, C.; Toropov, A. A.; Toropova, A. P.; Benfenati, E. QSAR Model for

Predicting Cell Viability of Human Embryonic Kidney Cells Exposed to SiO2 Nanoparticles. *Chemosphere* **2016**, *144*, 995–1001. https://doi.org/10.1016/j.chemosphere.2015.09.086.

(11) Choi, J. S.; Ha, M. K.; Trinh, T. X.; Yoon, T. H.; Byun, H. G. Towards a Generalized Toxicity Prediction Model for Oxide Nanomaterials Using Integrated Data from Different Sources. *Sci. Rep.* **2018**, *8*, 6110. https://doi.org/10.1038/s41598-018-24483-z.

(12) Fortino, V.; Kinaret, P. A. S.; Fratello, M.; Serra, A.; Saarimäki, L. A.; Gallud, A.; Gupta, G.; Vales, G.; Correia, M.; Rasool, O.; Ytterberg, J.; Monopoli, M.; Skoog, T.; Ritchie, P.; Moya, S.; Vázquez-Campos, S.; Handy, R.; Grafström, R.; Tran, L.; Zubarev, R.; Lahesmaa, R.; Dawson, K.; Loeschner, K.; Larsen, E. H.; Krombach, F.; Norppa, H.; Kere, J.; Savolainen, K.; Alenius, H.; Fadeel, B.; Greco, D. Biomarkers of Nanomaterials Hazard from Multi-Layer Data. *Nat. Commun.* **2022**, *13*. https://doi.org/10.1038/s41467-022-31609-5.

(13) Walkey, C. D.; Olsen, J. B.; Song, F.; Liu, R.; Guo, H.; Olsen, D. W. H.; Cohen, Y.; Emili, A.; Chan, W. C. W. Protein Corona Fingerprinting Predicts the Cellular Interaction of Gold and Silver Nanoparticles. *ACS Nano* **2014**, *8*, 2439–2455. https://doi.org/10.1021/nn406018q.

(14) Chen, R.; Zhang, Y.; Darabi Sahneh, F.; Scoglio, C. M.; Wohlleben, W.; Haase, A.; Monteiro-Riviere, N. A.; Riviere, J. E. Nanoparticle Surface Characterization and Clustering through Concentration-Dependent Surface Adsorption Modeling. *ACS Nano* **2014**, *8*, 9446–9456. https://doi.org/10.1021/nn503573s.

(15) Ho, S. Y.; Phua, K.; Wong, L.; Bin Goh, W. W. Extensions of the External Validation for Checking Learned Model Interpretability and Generalizability. *Patterns* **2020**, *1*, 100129. https://doi.org/10.1016/j.patter.2020.100129.

(16) Steckler, A.; McLeroy, K. R. The Importance of External Validity. *Am. J. Public Health* **2008**, *98*, 9–10. https://doi.org/10.2105/AJPH.2007.126847.

(17) Bleeker, S. E.; Moll, H. A.; Steyerberg, E. W.; Donders, A. R. T.; Derksen-Lubsen, G.; Grobbee, D. E.; Moons, K. G. M. External Validation Is Necessary in Prediction Research: A Clinical Example. *J. Clin. Epidemiol.* **2003**, *56*, 826–832. https://doi.org/10.1016/S0895-4356(03)00207-5.

(18) Monopoli, M. P.; Åberg, C.; Salvati, A.; Dawson, K. A. Biomolecular Coronas Provide the Biological Identity of Nanosized Materials. *Nat. Nanotechnol.* **2012**, *7*, 779–786. https://doi.org/10.1038/nnano.2012.207.

(19) Fytianos, G.; Rahdar, A.; Kyzas, G. Z. Nanomaterials in Cosmetics: Recent Updates. *Nanomaterials* **2020**, *10*, 979. https://doi.org/10.3390/nano10050979.

(20) Mebert, A. M.; Baglole, C. J.; Desimone, M. F.; Maysinger, D. Nanoengineered Silica: Properties, Applications and Toxicity. *Food Chem. Toxicol.* **2017**, *109*, 753–770. https://doi.org/10.1016/j.fct.2017.05.054.

(21) Miyata, T.; Nagao, T.; Watanabe, D.; Kumagai, A.; Akutagawa, K.; Morita, H.; Jinnai, H. Nanoscale Stress Distribution in Silica-Nanoparticle-Filled Rubber as Observed by Transmission Electron Microscopy: Implications for Tire Application. *ACS Appl. Nano Mater.* **2021**, *4*, 4452–4461. https://doi.org/10.1021/acsanm.1c00009.

(22) Mizutani, T.; Arai, K.; Miyamoto, M.; Kimura, Y. Application of Silica-Containing Nano-Composite Emulsion to Wall Paint: A New Environmentally Safe Paint of High Performance. *Prog. Org. Coatings* **2006**, *55*, 276–283. https://doi.org/10.1016/j.porgcoat.2005.12.001.

(23) Bernauer, U.; Bodin, L.; Chaudhry, Q.; Coenraads, P. J.; Dusinska, M.; Gaffet, E.; Panteri, E.; Rogiers, V.; Rousselle, C.; Stepnik, M.; Vanhaecke, T.; Wijnhoven, S.; von Goetz, N.; de Jong, W. H. The SCCS Scientific Advice on the Safety of Nanomaterials in Cosmetics. *Regul. Toxicol. Pharmacol.* **2021**, *126*, 105046. https://doi.org/10.1016/j.yrtph.2021.105046.

(24) Croissant, J. G.; Butler, K. S.; Zink, J. I.; Brinker, C. J. Synthetic Amorphous Silica Nanoparticles: Toxicity, Biomedical and Environmental Implications. *Nat. Rev. Mater.* **2020**, *5*, 886–909. https://doi.org/10.1038/s41578-020-0230-0.

(25) Murugadoss, S.; Lison, D.; Godderis, L.; Van Den Brule, S.; Mast, J.; Brassinne, F.; Sebaihi, N.; Hoet, P. H. Toxicology of Silica Nanoparticles: An Update. *Arch. Toxicol.* **2017**, *91*, 2967–3010. https://doi.org/10.1007/s00204-017-1993-y.

(26) Napierska, D.; Thomassen, L. C. J.; Lison, D.; Martens, J. A.; Hoet, P. H. The Nanosilica Hazard: Another Variable Entity. *Part. Fibre Toxicol.* **2010**, *7*, 39. https://doi.org/10.1186/1743-8977-7-39.

(27) Biological Evaluation of Medical Devices – Part 5: Tests for in Vitro Cytotoxicity. ISO 10993-5. Available at: Https://Www.Iso.Org/Obp/Ui/#iso:Std:Iso:10993:-5:En. **2009**. (Accessed: December 1, 2022)

(28) Regulation (EU) 2017/745 of the European Parliament and of the Council of 5 April 2017 on Medical Devices, Amending Directive 2001/83/EC, Regulation (EC) No 178/2002 and

Regulation (EC) No 1223/2009 and Repealing Council Directives 90/385/EEC and 93/42/EE.

(29) Dong, X.; Wu, Z.; Li, X.; Xiao, L.; Yang, M.; Li, Y.; Duan, J.; Sun, Z. The Size-Dependent Cytotoxicity of Amorphous Silica Nanoparticles: A Systematic Review of in Vitro Studies. *Int. J. Nanomedicine* **2020**, *15*, 9089–9113. https://doi.org/10.2147/IJN.S276105.

(30) Lundberg, S. M.; Erion, G.; Chen, H.; DeGrave, A.; Prutkin, J. M.; Nair, B.; Katz, R.; Himmelfarb, J.; Bansal, N.; Lee, S. I. From Local Explanations to Global Understanding with Explainable AI for Trees. *Nat. Mach. Intell.* **2020**, *2*, 56–67. https://doi.org/10.1038/s42256-019-0138-9.

(31) Cawley, G. C.; Talbot, N. L. C. On Over-Fitting in Model Selection and Subsequent Selection Bias in Performance Evaluation. *J. Mach. Learn. Res.* **2010**, *11*, 2079–2107.

(32) Kim, W.; Kim, W. K.; Lee, K.; Son, M. J.; Kwak, M.; Chang, W. S.; Min, J. K.; Song, N. W.; Lee, J.; Bae, K. H. A Reliable Approach for Assessing Size-Dependent Effects of Silica Nanoparticles on Cellular Internalization Behavior and Cytotoxic Mechanisms. *Int. J. Nanomedicine* **2019**, *14*, 7375–7387. https://doi.org/10.2147/IJN.S224183.

(33) Blechinger, J.; Bauer, A. T.; Torrano, A. A.; Gorzelanny, C.; Bräuchle, C.; Schneider, S. W. Uptake Kinetics and Nanotoxicity of Silica Nanoparticles Are Cell Type Dependent. *Small* **2013**, *9*, 3970–3980. https://doi.org/10.1002/smll.201301004.

(34) Lesniak, A.; Fenaroli, F.; Monopoli, M. P.; Åberg, C.; Dawson, K. A.; Salvati, A. Effects of the Presence or Absence of a Protein Corona on Silica Nanoparticle Uptake and Impact on Cells. *ACS Nano* **2012**, *6*, 5845–5857. https://doi.org/10.1021/nn300223w.

(35) Lesniak, A.; Salvati, A.; Santos-Martinez, M. J.; Radomski, M. W.; Dawson, K. A.; Åberg, C. Nanoparticle Adhesion to the Cell Membrane and Its Effect on Nanoparticle Uptake Efficiency. *J. Am. Chem. Soc.* **2013**, *135*, 1438–1444. https://doi.org/10.1021/ja309812z.

(36) Francia, V.; Yang, K.; Deville, S.; Reker-Smit, C.; Nelissen, I.; Salvati, A. Corona Composition Can Affect the Mechanisms Cells Use to Internalize Nanoparticles. *ACS Nano* **2019**, *13*, 11107–11121. https://doi.org/10.1021/acsnano.9b03824.

(37) Pavan, C.; Santalucia, R.; Leinardi, R.; Fabbiani, M.; Yakoub, Y.; Uwambayinema, F.; Ugliengo, P.; Tomatis, M.; Martra, G.; Turci, F.; Lison, D.; Fubini, B. Nearly Free Surface Silanols Are the Critical Molecular Moieties That Initiate the Toxicity of Silica Particles. *Proc. Natl. Acad. Sci. U. S. A.* **2020**, *117*, 27836–27846. https://doi.org/10.1073/pnas.2008006117.

(38) Tenzer, S.; Docter, D.; Kuharev, J.; Musyanovych, A.; Fetz, V.; Hecht, R.; Schlenk, F.; Fischer,

D.; Kiouptsi, K.; Reinhardt, C.; Landfester, K.; Schild, H.; Maskos, M.; Knauer, S. K.; Stauber, R. H. Rapid Formation of Plasma Protein Corona Critically Affects Nanoparticle Pathophysiology. *Nat. Nanotechnol.* **2013**, *8*, 772–781. https://doi.org/10.1038/nnano.2013.181.

(39) Zhang, H.; Dunphy, D. R.; Jiang, X.; Meng, H.; Sun, B.; Tarn, D.; Xue, M.; Wang, X.; Lin, S.; Ji, Z.; Li, R.; Garcia, F. L.; Yang, J.; Kirk, M. L.; Xia, T.; Zink, J. I.; Nel, A.; Brinker, C. J. Processing Pathway Dependence of Amorphous Silica Nanoparticle Toxicity: Colloidal vs Pyrolytic. *J. Am. Chem. Soc.* **2012**, *134*, 15790–15804. https://doi.org/10.1021/ja304907c.

(40) Prokhorenkova, L.; Gusev, G.; Vorobev, A.; Dorogush, A. V.; Gulin, A. Catboost: Unbiased Boosting with Categorical Features. *Adv. Neural Inf. Process. Syst.* **2018**, *2018-Decem*, 6638–6648.

(41) Schardt, C.; Adams, M. B.; Owens, T.; Keitz, S.; Fontelo, P. Utilization of the PICO Framework to Improve Searching PubMed for Clinical Questions. *BMC Med. Inform. Decis. Mak.* **2007**, *7*, 16. https://doi.org/10.1186/1472-6947-7-16.

(42) Marin, F.; Rohatgi, A.; Charlot, S. WebPlotDigitizer, a Polyvalent and Free Software to Extract Spectra from Old Astronomical Publications: Application to Ultraviolet Spectropolarimetry. *arXiv[Preprint]* **2017**. 1708.02025. https://arxiv.org/abs/1708.02025 (Accessed: December 1, 2022)

(43) Gong, C.; Yang, L.; Zhou, J.; Guo, X.; Zhuang, Z. Possible Role of PAPR-1 in Protecting Human HaCaT Cells against Cytotoxicity of SiO2 Nanoparticles. *Toxicol. Lett.* **2017**, *280*, 213–221. https://doi.org/10.1016/j.toxlet.2017.07.213.

(44) Liu, W.; Hu, T.; Zhou, L.; Wu, D.; Huang, X.; Ren, X.; Lv, Y.; Hong, W.; Huang, G.; Lin, Z.; Liu, J. Nrf2 Protects against Oxidative Stress Induced by SiO2 Nanoparticles. *Nanomedicine* **2017**, *12*, 2303–2318. https://doi.org/10.2217/nnm-2017-0046.

(45) Nishijima, N.; Hirai, T.; Misato, K.; Aoyama, M.; Kuroda, E.; Ishii, K. J.; Higashisaka, K.; Yoshioka, Y.; Tsutsumi, Y. Human Scavenger Receptor A1-Mediated Inflammatory Response to Silica Particle Exposure Is Size Specific. *Front. Immunol.* **2017**, *8*, 1–12. https://doi.org/10.3389/fimmu.2017.00379.

(46) Premshekharan, G.; Nguyen, K.; Zhang, H.; Forman, H. J.; Leppert, V. J. Low Dose Inflammatory Potential of Silica Particles in Human-Derived THP-1 Macrophage Cell Culture Studies – Mechanism and Effects of Particle Size and Iron. *Chem. Biol. Interact.* **2017**, *272*,

160–171. https://doi.org/10.1016/j.cbi.2017.05.004.

(47) Vicente, S.; Moia, C.; Zhu, H.; Vigé, X. In Vitro Evaluation of the Internalization and Toxicological Profile of Silica Nanoparticles and Submicroparticles for the Design of Dermal Drug Delivery Strategies. *J. Appl. Toxicol.* **2017**, *37*, 1396–1407. https://doi.org/10.1002/jat.3507.

(48) Kusaczuk, M.; Krętowski, R.; Naumowicz, M.; Stypułkowska, A.; Cechowska-Pasko, M. Silica Nanoparticle-Induced Oxidative Stress and Mitochondrial Damage Is Followed by Activation of Intrinsic Apoptosis Pathway in Glioblastoma Cells. *Int. J. Nanomedicine* **2018**, *13*, 2279–2294. https://doi.org/10.2147/IJN.S158393.

(49) Zang, X. M.; Li, J. M.; Wang, Y.; Liu, Y. Y.; Wei, Z. B.; Yang, L.; Miao, A. J. A Facile Method to Study the Bioaccumulation Kinetics of Amorphous Silica Nanoparticles by Quantum Dot Embedding. *Environ. Sci. Nano* **2018**, *5*, 2830–2841. https://doi.org/10.1039/c8en00387d.

(50) Du, Q.; Ge, D.; Mirshafiee, V.; Chen, C.; Li, M.; Xue, C.; Ma, X.; Sun, B. Assessment of Neurotoxicity Induced by Different-Sized Stöber Silica Nanoparticles: Induction of Pyroptosis in Microglia. *Nanoscale* **2019**, *11*, 12965–12972. https://doi.org/10.1039/c9nr03756j.

(51) Kamikubo, Y.; Yamana, T.; Hashimoto, Y.; Sakurai, T. Induction of Oxidative Stress and Cell Death in Neural Cells by Silica Nanoparticles. *ACS Chem. Neurosci.* **2019**, *10*, 304–312. https://doi.org/10.1021/acschemneuro.8b00248.

(52) Lee, K.; Lee, J.; Kwak, M.; Cho, Y. L.; Hwang, B.; Cho, M. J.; Lee, N. G.; Park, J.; Lee, S. H.; Park, J. G.; Kim, Y. G.; Kim, J. S.; Han, T. S.; Cho, H. S.; Park, Y. J.; Lee, S. J.; Lee, H. G.; Kim, W. K.; Jeung, I. C.; Song, N. W. *et al*. Two Distinct Cellular Pathways Leading to Endothelial Cell Cytotoxicity by Silica Nanoparticle Size. *J. Nanobiotechnology* **2019**, *17*, 24. https://doi.org/10.1186/s12951-019-0456-4.

(53) Ren, L.; Liu, J.; Zhang, J.; Wang, J.; Wei, J.; Li, Y.; Guo, C.; Sun, Z.; Zhou, X. Silica Nanoparticles Induce Spermatocyte Cell Autophagy through MicroRNA-494 Targeting AKT in GC-2spd Cells. *Environ. Pollut.* **2019**, *255*, 113172. https://doi.org/10.1016/j.envpol.2019.113172.

(54) Crucho, C. I. C.; Avó, J.; Nobuyasu, R.; N. Pinto, S.; Fernandes, F.; Lima, J. C.; Berberan-Santos, M. N.; Dias, F. B. Silica Nanoparticles with Thermally Activated Delayed Fluorescence for Live Cell Imaging. *Mater. Sci. Eng. C* **2020**, *109*, 110528. https://doi.org/10.1016/j.msec.2019.110528.

(55) Liu, Y.; Wei, H.; Tang, J.; Yuan, J.; Wu, M.; Yao, C.; Hosoi, K.; Yu, S.; Zhao, X.; Han, Y.; Chen, G. Dysfunction of Pulmonary Epithelial Tight Junction Induced by Silicon Dioxide Nanoparticles via the ROS/ERK Pathway and Protein Degradation. *Chemosphere* **2020**, *255*, 126954. https://doi.org/10.1016/j.chemosphere.2020.126954.

(56) Nazarparvar-Noshadi, M.; Ezzati Nazhad Dolatabadi, J.; Rasoulzadeh, Y.; Mohammadian, Y.; Shanehbandi, D. Apoptosis and DNA Damage Induced by Silica Nanoparticles and Formaldehyde in Human Lung Epithelial Cells. *Environ. Sci. Pollut. Res.* **2020**, *27*, 18592–18601. https://doi.org/10.1007/s11356-020-08191-8.

(57) Tada-Oikawa, S.; Eguchi, M.; Yasuda, M.; Izuoka, K.; Ikegami, A.; Vranic, S.; Boland, S.; Tran, L.; Ichihara, G.; Ichihara, S. Functionalized Surface-Charged Sio2 Nanoparticles Induce pro-Inflammatory Responses, but Are Not Lethal to Caco-2 Cells. *Chem. Res. Toxicol.* **2020**, *33*, 1226–1236. https://doi.org/10.1021/acs.chemrestox.9b00478.

(58) Wang, M.; Li, J.; Dong, S.; Cai, X.; Cai, X.; Simaiti, A.; Yang, X.; Zhu, X.; Zhu, X.; Luo, J.; Jiang, L. H.; Jiang, L. H.; Du, B.; Yu, P.; Yang, W. Silica Nanoparticles Induce Lung Inflammation in Mice via ROS/PARP/TRPM2 Signaling-Mediated Lysosome Impairment and Autophagy Dysfunction. *Part. Fibre Toxicol.* **2020**, *17*, 1–22. https://doi.org/10.1186/s12989-020-00353-3.

(59) Cui, G.; Li, Z.; Cao, F.; Li, P.; Jin, M.; Hou, S.; Yang, X.; Mu, Y.; Peng, C.; Shao, H.; Du, Z. Activation of Nrf2/HO-1 Signaling Pathway Attenuates ROS-Mediated Autophagy Induced by Silica Nanoparticles in H9c2 Cells. *Environ. Toxicol.* **2021**, *36*, 1389–1401. https://doi.org/10.1002/tox.23134.

(60) Hou, S.; Zhang, X.; Du, H.; Ning, X.; Wu, H.; Li, C.; Liu, Y.; Sun, Z.; Du, Z.; Jin, M. Silica Nanoparticles Induce Mitochondrial Pathway-Dependent Apoptosis by Activating Unfolded Protein Response in Human Neuroblastoma Cells. *Environ. Toxicol.* **2021**, *36*, 675–685. https://doi.org/10.1002/tox.23071.

(61) Ruan, C.; Wang, C.; Gong, X.; Zhang, Y.; Deng, W.; Zhou, J.; Huang, D.; Wang, Z.; Zhang, Q.; Guo, A.; Lu, J.; Gao, J.; Peng, D.; Xue, Y. An Integrative Multi-Omics Approach Uncovers the Regulatory Role of CDK7 and CDK4 in Autophagy Activation Induced by Silica Nanoparticles. *Autophagy* **2021**, *17*, 1426–1447. https://doi.org/10.1080/15548627.2020.1763019.

(62) Hou, S.; Li, C.; Wang, Y.; Sun, J.; Guo, Y.; Ning, X.; Ma, K.; Li, X.; Shao, H.; Cui, G.; Jin, M.; Du, Z. Silica Nanoparticles Cause Activation of NLRP3 Inflammasome In-Vitro Model-Using

Microglia. *Int. J. Nanomedicine* **2022**, *Volume 17*, 5247–5264. https://doi.org/10.2147/ijn.s372485.

(63) Kim, I. Y.; Choi, J. W.; Kwon, I. H.; Hwangbo, S.; Bae, S. H.; Kwak, M.; Kim, J.; Lee, T. G.; Heo, M. B. Variations in in Vitro Toxicity of Silica Nanoparticles According to Scaffold Type in a 3D Culture System Using a Micropillar/Microwell Chip Platform. *Sensors Actuators B Chem.* **2022**, *369*, 132328. https://doi.org/10.1016/j.snb.2022.132328.

(64) Liang, Q.; Ma, Y.; Wang, F.; Sun, M.; Lin, L.; Li, T.; Sun, Z.; Duan, J. Silica Nanoparticles Induce Hepatocyte Ferroptosis and Liver Injury via Ferritinophagy. *Environ. Sci. Nano* **2022**, *9*, 3014–3029. https://doi.org/10.1039/d2en00116k.

(65) Ma, Y.; Liang, Q.; Wang, F.; Yan, K.; Sun, M.; Lin, L.; Li, T.; Duan, J.; Sun, Z. Silica Nanoparticles Induce Pulmonary Autophagy Dysfunction and Epithelial-to-Mesenchymal Transition via P62/NF-KB Signaling Pathway. *Ecotoxicol. Environ. Saf.* **2022**, *232*. https://doi.org/10.1016/j.ecoenv.2022.113303.

(66) Zhang, Z.; Zhao, L.; Ma, Y.; Liu, J.; Huang, Y.; Fu, X.; Peng, S.; Wang, X.; Yang, Y.; Zhang, X.; Ding, W.; Yu, J.; Zhu, Y.; Yan, H.; Yang, S. Mechanistic Study of Silica Nanoparticles on the Size-Dependent Retinal Toxicity in Vitro and in Vivo. *J. Nanobiotechnology* **2022**, *20*, 1–19. https://doi.org/10.1186/s12951-022-01326-8.

(67) Hirai, T.; Yoshioka, Y.; Takahashi, H.; Ichihashi, K. ichi; Udaka, A.; Mori, T.; Nishijima, N.; Yoshida, T.; Nagano, K.; Kamada, H.; Tsunoda, S. I.; Takagi, T.; Ishii, K. J.; Nabeshi, H.; Yoshikawa, T.; Higashisaka, K.; Tsutsumi, Y. Cutaneous Exposure to Agglomerates of Silica Nanoparticles and Allergen Results in IgE-Biased Immune Response and Increased Sensitivity to Anaphylaxis in Mice. *Part. Fibre Toxicol.* **2015**, *12*, 1–6. https://doi.org/10.1186/s12989-015-0095-3.

(68) Nabeshi, H.; Yoshikawa, T.; Matsuyama, K.; Nakazato, Y.; Matsuo, K.; Arimori, A.; Isobe, M.; Tochigi, S.; Kondoh, S.; Hirai, T.; Akase, T.; Yamashita, T.; Yamashita, K.; Yoshida, T.; Nagano, K.; Abe, Y.; Yoshioka, Y.; Kamada, H.; Imazawa, T.; Itoh, N. *et al*. Systemic Distribution, Nuclear Entry and Cytotoxicity of Amorphous Nanosilica Following Topical Application. *Biomaterials* **2011**, *32*, 2713–2724. https://doi.org/10.1016/j.biomaterials.2010.12.042.

(69) Lundberg, S. M.; Lee, S. I. A Unified Approach to Interpreting Model Predictions Scott. *Adv. Neural Inf. Process. Syst. 30* **2017**, *30*, 4768–4777.

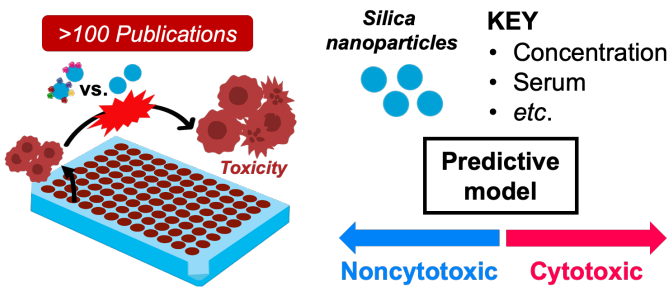

TOC graphic (For Table of Contents Only)